

DEPARTMENT OF THEORETICAL PHYSICS AND COMPUTER MODELLING

Head of Department *Dr. hab. phys.* Eugene Kotomin

Research Area and Main Problems

Our theoretical research interests are focused on six classes of problems related to:

- kinetics of diffusion-controlled processes, with emphasis on pattern formation and catalytic surface reactions;
- the atomic and electronic structure of numerous advanced materials, with emphasis on calculations of properties of defects, surfaces, metal/insulator interfaces;
- theoretical simulations and experimental studies of nanostructures and nanomaterials, *e.g.*, evaluation of their photocatalytic suitability;
- modeling of advanced functional materials for energy applications (fuel cells, ceramic membranes, Li batteries, fusion and fission reactors);
- gyrotron development for thermonuclear reactors

We combine several different techniques, including analytical formalisms and large-scale computer simulations (quantum chemical methods, stochastic simulations as well as Monte Carlo/cellular automata modeling) as described in our homepage <http://www1.cfi.lu.lv/teor>

Staff

Laboratory of kinetics in self-organizing systems	Laboratory of computer modeling of electronic structure of solids
Dr. O. Dumbrajs (full member of Latvian Acad. Sci.)	Dr. D. Bocharov
Dr. D. Gryaznov	Dr. R. Eglitis (corr. member of Latvian Acad.Sci.)
Dr. E. Klotins	Dr. Yu. Mastrikov
Dr. hab. E. Kotomin (full member of Latvian Acad. Sci.)	Dr. S. Piskunov
Dr. hab. V. Kuzovkov	Dr. hab. Yu. Shunin
Dr. A. Popov	Dr. Yu. Zhukovskii
Dr. G. Zvejnieks	M.S. A. Chesnokov
M.S. J. Shirmane	M.S. A. Gopejenko
B.S. Moskina	M.S. J. Kazerovskis
	M.S. B.S. O. Lisovski
	M.S. A. Platonenko
	B.S. M. Sokolov

Scientific visits abroad

1. Dr. hab. E. Kotomin, Max-Planck Institut für Festkörperforschung, Stuttgart, Germany (8 months), Photochemistry Center, Russian Academy of Sciences, Moscow, Russia (1 week)
2. Dr. O. Dumbrajs, Fukui University, Japan (3 months)
3. Dr. A. Popov, Max Planck Institute, Stuttgart, Germany (1 week); Institute of Physics, University of Tartu, Estonia (3 weeks), CIEMAT, Spain (1 week)
4. Dr. D. Bocharov, Paul Scherrer Institut, Viligen, Switzerland (8 months), University of Duisburg-Essen, Germany (two weeks)
5. Dr. Yu. Mastrikov, Institut für Angewandte Materialien, Karlsruhe Institut für Technologie, Germany (2 weeks)
6. Dr. S. Piskunov, University of Duisburg-Essen, Germany (two months)
7. Dr. hab. Yu. Shunin, Laboratori Nazionali di Frascati, Italy (1 month)
8. Dr. Yu. Zhukovskii, St. Petersburg State University, Russia (3 weeks), Institut für Angewandte Materialien, Karlsruhe Institut für Technologie, Germany (2 weeks)
9. M.S. A. Gopejenko, Institut für Angewandte Materialien, Karlsruhe Institut für Technologie, Germany (one month)
10. M.S. A. Chesnokov, University of Duisburg-Essen, Germany (2 weeks)
11. M.S. J. Kazerovskis, University of Ulm, Germany (10 months)
12. M.S. O. Lisovski, Uppsala University, Sweden (7 months)

International Cooperation

Belarus	1. Institute of Nuclear Problems, Belarusian State University, Minsk (Prof. S. A. Maksimenko)
China	2. Beijing Institute of Technology, Beijing (Dr. H. Shi).
Estonia	3. Institute of Physics, University of Tartu (Prof. A. Lushchik)
Finland	4. Helsinki University of Technology, Espoo (Dr. T. Kurki-Suonio)
France	5. Laue-Langevin Institute, Grenoble, Prof. H. Schober)
Germany	6. Max Planck Institut für Festkörperforschung, Stuttgart (Prof. Dr. J. Maier)
	7. Deutsches Elektronen-Synchrotron DESY, Hamburg (Dr. A. Kotlov)
	8. Darmstadt University of Technology, Darmstadt (Prof. H von Seggern)
	9. Institut für Hochleistungsimpuls & Mikrowellentechnik (KIT), Karlsruhe (Dr. S. Kern, Dr. B. Piosczyk)
	10. Max-Planck Institut für Plasmaphysik, Garching, (Prof. Dr. H. Zohm)
Israel	11. Institut für Angewandte Materialien (KIT), Karlsruhe (Prof. Dr. A. Möslang, Dr. P. Vladimirov)
	12. Dept Theoretical Chemistry, Univ. Duisburg-Essen (Prof. Dr. E. Spohr)
Italy	13. Ben Gurion University, Beer Sheva (Prof. D. Fuks)
Kazakhstan	14. Laboratori Nazionali di Frascati (Dr. S. Bellucci, Dr. M. Cestelli-Guidi)
	15. Gumilyov Eurasian National University, Astana (Prof. A.T. Akilbekov)
Japan	16. FIR Center, University of Fukui (Prof. T. Idehara)

Lithuania	17. Institute of Semiconductor Physics (SPI), Vilnius (Dr. E. Tornau)
Norway	18. Center for Materials Science and Nanotechnology, Department of Chemistry, University of Oslo, FASE, Norway
Poland	19. Warsaw University, Department of Chemistry (Prof. A. Huczko, Prof. A. Dąbrowska)
	20. Institute of Physics, Academy of Science, Warsaw (Prof. H. Szymczak)
Romania	21. University of Craiova (Dr. D. Constantinescu)
	22. St. Petersburg State University, Petrodvorets (St. Petersburg) (Prof. R.A. Evarestov)
Russia	23. Institute of General and Inorganic Chemistry, Russian Academy of Sciences, Moscow (Prof. P.N. Dyachkov)
	24. Photochemistry Center, Russian Academy of Sciences, Moscow (Prof. A.A. Bagaturyants)
Spain	25. Centro de Investigaciones Energeticas Medioambientales y Tecnologicas (CIEMAT), Madrid (Dr. R. Vila)
UK	26. University College London (Prof. A.L. Shluger)
Ukraine	27. Ivan Franko National University, Lviv (Prof. O. I. Aksimentyeva, Prof. I. Bolesta, Dr. I. Karbovnyk)
USA	28. University of Maryland, College Park (Dr. G.S. Nusinovich, Dr. M.M. Kukla)

Main Results

A. Electronic structure calculations for advanced materials

Thermodynamic stability of stoichiometric BiFeO₃

E.A. Kotomin,

E. Heifets, R. Merkle, J. Maier

Max Planck Institute for Solid State Research, Stuttgart, Germany

BiFeO₃ (BFO) continues to attract great attention due to its multiferroic properties under ambient conditions. It was found also, that photocatalytic and photovoltaic properties of BFO are enhanced due to its ferroelectricity. Related perovskite solid solutions (Bi_{1-x}Sr_xFeO_{3-δ} and Bi_{1-x}Sr_xFe_{1-y}Co_yO_{3-δ}) were proposed recently as cathodes for solid oxide fuel cells (SOFCs) operating at intermediate temperatures (> 600 °C). Determination of thermodynamic stability conditions for BFO is important and represents the first step for future investigations of formation of intrinsic defects, surface structures and surface chemical reactions (e.g. oxygen reduction reaction), as well as formation of solid solutions, like the mentioned above cathode materials, their possible structures and stability. Also, the data on stability of BFO can be used to provide valuable information on conditions suitable to produce this and related materials. Based on first principles hybrid calculations performed *in close collaboration with Max Planck Institute for Solid State Research, Stuttgart* the phase diagram has been constructed (**Fig. 1**), which allows us to predict the stability region of stoichiometric BiFeO₃.

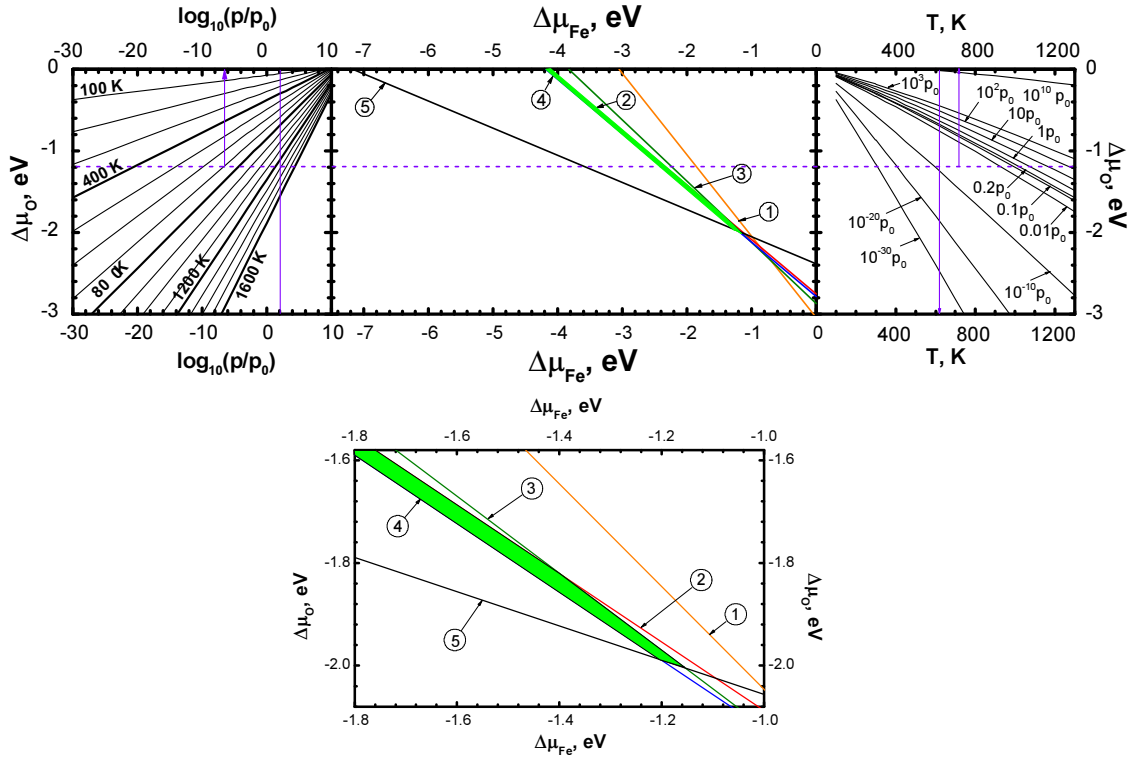


Figure 1. (a) Phase diagrams for BiFeO_3 based on hybrid density functional calculations with all electrons on Fe ions included explicitly. The numbered lines in the central panel describe conditions of forming of: 1) FeO ; 2) Fe_2O_3 ; 3) Fe_3O_4 ; 4) Bi_2O_3 ; 5) Bi metal. Green area marks the region of BiFeO_3 stability. Side panels serve to convert values of oxygen chemical potential to easily observable values of temperature T and oxygen partial pressure p_{O_2} . (b) Enlargement of the region marked by a rectangular from (a). for more details on applied technique. The variation of chemical potential for Fe atoms is defined as the deviation of Fe atoms chemical potential from value in metallic iron ($\Delta\mu_{\text{Fe}} \approx \mu_{\text{Fe}} - E_{\text{Fe}}$), which is the standard state for the iron and approximated by the total energy of Fe atom in Fe metal. Similarly, the variation of O atom chemical potential is calculated with respect to the total energy of O atom in O_2 molecule

Thermodynamic properties of neutral and charged oxygen vacancies in BaZrO_3 based on first principles phonon calculations

D. Gryaznov, E.A. Kotomin

M. Arrigoni, J. Maier

Max Planck Institute for Solid State Research, Heisenbergstrasse 1, Stuttgart, Germany

T. S. Bjørheim

Centre for Materials Science and Nanotechnology, Department of Chemistry, University of Oslo, FASE, Norway

ABO_3 -type perovskite structured oxides comprise a broad family of technologically important materials, which display a wide range of functional properties, such as ferroelectricity, magnetism, their combination (multiferroics), piezoelectricity, high-temperature superconductivity, mixed ionic-electronic conductivity and electro-optic effects. Oxygen vacancies are common point defects in these materials and were shown to influence a variety of properties, *e.g.*, mechanical and optical properties, as well as ionic conductivity.

The structural, electronic and thermodynamic properties of neutral (v_{O}^{\times}) and positively doubly charged (v_{O}^{2+}) oxygen vacancies in the BaZrO_3 are addressed by first principles phonon calculations (Fig. 2). The calculations have been performed *in close collaboration with Max Planck Institute for Solid State Research, Stuttgart, and Centre for Materials Science and Nanotechnology, University of Oslo*, using two complementary first principles approaches and functionals; the linear combination of atomic orbitals (LCAO) within hybrid Hartree-Fock and density functional theory formalism (HF-DFT), and the projector augmented plane wave approach (PAW) within DFT and PW basis set. Phonons are shown to contribute significantly to the formation energy of the charged oxygen vacancy at high temperatures (~ 1 eV at 1000 K), due to both its large distortion of the local structure, and its large negative formation volume. For the neutral vacancy the resulting lattice distortions, and thus the contributions from phonons to the free formation energy, are significantly smaller. As a result, phonons affect the relative stability of the two defects at finite temperatures and the charge transition level for oxygen vacancies ($+2/0$) is predicted change from 0.42 to 0.83 eV below the conduction band bottom as temperature increases from 0 K to 1000 K.

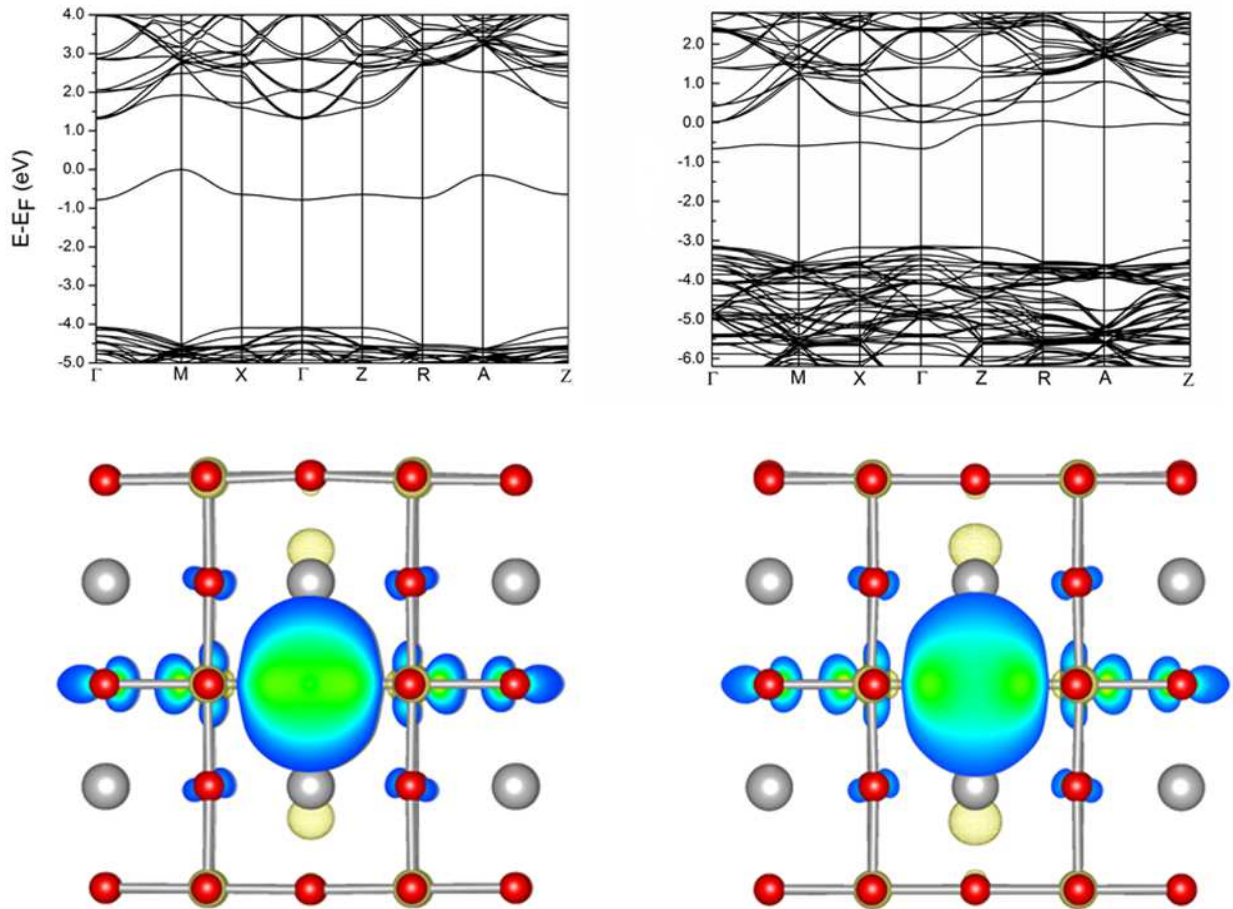


Figure 2 Top: Band structure of the $2 \times 2 \times 2$ BaZrO_3 supercell with a v_{O}^{\times} calculated with CRYSTAL (left) and VASP (right); bottom: electronic charge density of v_{O}^{\times} projected on the defect level obtained with CRYSTAL using the ghost BS (left) or leaving vacuum (right). The isosurface threshold level is set to $0.002 e/a_0^3$; only points with an electron charge density value greater than the threshold are shown and they lie inside the isosurface (the larger the value, the warmer the color).

Hydration Entropy of BaZrO₃: First Principles Phonon Calculations

E.A. Kotomin,

T. S. Bjørheim

Center for Mater. Science and Nanotechnology, Department of Chemistry, University of Oslo, FERMIo, Norway

R. Merkle, J. Maier

Max Planck Institute for Solid State Research, Stuttgart, Germany

Oxide crystals display solid state protonic conduction at temperatures up to 1000 °C, and may thus be used as electrolytes in the intermediate temperature solid oxide fuel cells, electrolyzers and H₂ gas separation membranes. Acceptor-doped barium zirconate, *e.g.*, BaZr_{1-x}Y_xO₃, is the most promising candidate material for practical applications to date, with a protonic conductivity of $\sim 10^{-2}$ S/cm at 600 °C.

The impact of phonons on the hydration and defect thermodynamics of undoped and acceptor (Sc, In, Y and Gd) doped BaZrO₃ has addressed by means of first principles supercell calculations, *in collaboration with Max Planck Institute for Solid State Research, Stuttgart, and Centre for Materials Science and Nanotechnology, University of Oslo*. In contrast to previous, similar investigations, we evaluate contributions from all phonon modes, and also pressure/volume effects on the phonon properties. The calculations are performed at the GGA-level with the PBE and RPBE functionals, which both predict for BaZrO₃ a stable cubic perovskite structure (**Fig. 3**). Both functionals also give similar defect entropies for undoped, and Sc- and In-doped BaZrO₃. For all dopants, the vibrational formation entropy of the fully charged oxygen vacancy ($v_{\text{O}}^{\bullet\bullet}$) is significantly lower than that of the protonic defect ($\text{OH}_{\text{O}}^{\bullet}$), which therefore also is the dominant contribution to the entropy of hydration, in addition to loss of H₂O(g). The large, negative vibrational formation entropy of $v_{\text{O}}^{\bullet\bullet}$ stems both from local structural relaxations, and contraction of the entire supercell and corresponding blue-shift of the phonon spectrum. Neglect of the phonon contribution to the vacancy free formation energy leads to a significant error (120 kJ/mol at 1000 K). The formation volume and vibrational formation entropy of both $\text{OH}_{\text{O}}^{\bullet}$ and $v_{\text{O}}^{\bullet\bullet}$ become more negative with increasing dopant size. The calculated hydration entropies, and the trend of more negative entropies in the order Y < Gd < In < Sc, are in good agreement with experimental results, lending support to the applicability of the adopted method.

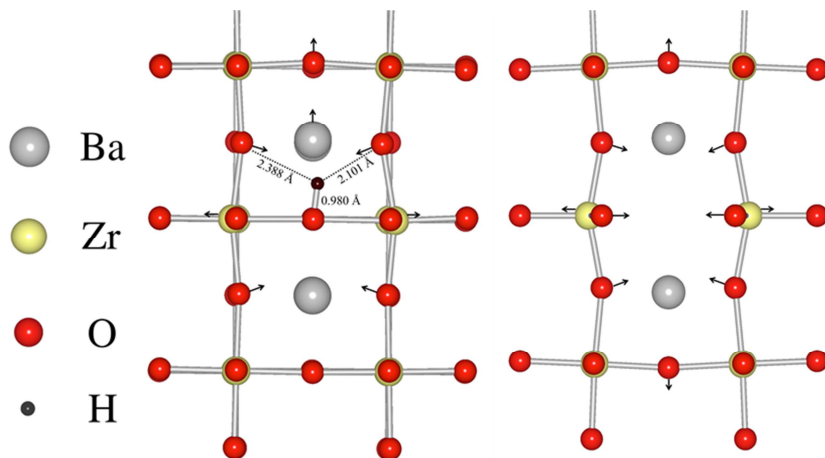


Figure 3. Atomic structure of $\text{OH}_{\text{O}}^{\bullet}$ and $v_{\text{O}}^{\bullet\bullet}$ in a $3 \times 3 \times 3$ supercell calculated with PBE and full volume relaxations. The structures are projected along the (0 0 1) direction and show the major atomic relaxations around the defects.

Water interaction with perfect and fluorine-doped Co_3O_4 (100) surface

Yu.A. Mastrikov, E.A. Kotomin

G.A. Kaptagay, T.M. Inerbaev, A.T. Akilbekov

L.N. Gumilyov Eurasian National University, Astana, Kazakhstan

The increasing consumption of energy has stimulated intensive research of different kinds of renewable energy resources. This includes research of spinel-type tri-cobalt tetra oxide (Co_3O_4) as a cathode material for water splitting at ambient temperatures as a result of the oxygen evolution reaction (OER). The interaction of H_2O with transition-metal oxide surfaces plays also important role in catalysis, surface chemistry, gas sensors, photochemistry, and electrochemistry. One of the main characteristics of the OER is the overpotential.

Whereas the atomic scale mechanisms of the OER is complicated and not fully studied, insights into the thermodynamics of the reaction can be obtained using the recently developed schemes based on the first principles calculations. Theoretical investigations of water adsorption on perfect and fluorine-doped Co_3O_4 (100) surface have been performed *in collaboration with L.N. Gumilyov Eurasian National University, Astana*, by means of the plane-wave periodic density functional theory (DFT) calculations combined with the Hubbard- U approach and statistical thermodynamics (**Fig. 4**). We demonstrated the positive effect of fluorine-doping of the Co_3O_4 (100) surface and calculated oxygen evolution reaction overpotential based on the Gibbs free-energy diagram of perfect and F-doped surfaces.

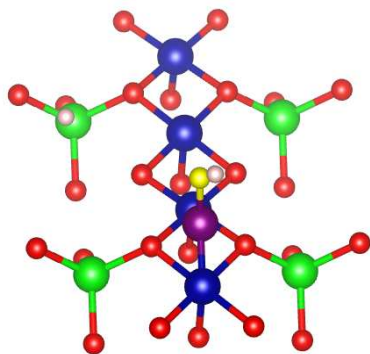


Figure 4. Top view of dissociation geometry on the Co_3O_4 (100) $\text{Co}_{0.5}$ -terminated surface. Color coding: Co_{5c}^o , blue; Co_{4c}^T , green; Co_{2c}^T , purple; water O, yellow; H atom, white.

C-, N-, S-, and Fe-doped TiO_2 and SrTiO_3 nanotubes for visible-light-driven photocatalytic water splitting: Prediction from first principles

A. Chesnokov, S. Piskunov, O. Lisovski, D. Bocharov, Yu.F. Zhukovskii

E. Spohr, M. Wessel

Department of Theoretical Chemistry, University of Duisburg-Essen, Germany

Water splitting under the influence of solar light on semiconducting electrodes inserted in aqueous electrolyte is a potentially clean and renewable source for production of hydrogen fuel. Its efficiency depends on relative position of the band gap edges (the visible light interval between infrared and ultraviolet ranges of electromagnetic spectrum corresponds to gap widths 1.5-2.8 eV) accompanied by a proper band alignment relative to both reduction (H^+/H_2) and oxidation ($\text{O}_2/\text{H}_2\text{O}$) potentials (4.44 eV and 5.67 eV, respectively) which must be positioned inside the band gap. Some metal oxides are capable of driving the water-splitting

reaction when irradiated with sunlight, and both titania and strontium titanate are among these materials. Band gaps of cubic perovskite-type SrTiO_3 and TiO_2 anatase-type bulk were experimentally found to be 3.2 eV for both materials, which corresponds to photocatalytic activity under ultraviolet light possessing only $\sim 1\%$ efficiency of sunlight energy conversion.

In collaboration with Department of Theoretical Chemistry, University of Duisburg-Essen, Germany, we have performed large-scale *ab initio* ground-state calculations on the single-wall anatase-structured $\text{TiO}_2(001)$ and cubic $\text{SrTiO}_3(110)$ nanotubes, with fixed number of atomic layers as well as chiral indexes $(n,0)$ for both NTs, respectively, doped by C, N, S, or Fe atoms and co-doped by pair of N and S atoms. We have constructed also both periodic and cluster models of doped TiO_2 NTs, for which either *CRYSTAL09* code or *NWChem* code have been applied, respectively. For both types of calculations, we have used the formalism of localised Gaussian-type functions (GTFs), which form the basis set (BS) of localised atomic orbitals for each chemical element as implemented in both types of codes where crystalline and molecular orbitals are constructed within either CO LCAO or MO LCAO approaches.

Noticeable growth of photocatalytic efficiency can be achieved by essential adjustment of band edges for titania bulk through nanoscale transformation of its morphology to anatase-type nanotubes formed by folding of nanosheet (001) TiO_2 sheets consisting of 9 atomic layers and six-layer (110) SrTiO_3 sheets, both possessing $(n,0)$ chiralities, accompanied by partial substitution of pristine atoms by C_O , Fe_Ti , N_O and S_O simple dopants as well as $\text{N}_\text{O}+\text{S}_\text{O}$ co-dopant (in the case of TiO_2 NTs). In the former case, the band gap can be reduced down to 2.2 eV (**Fig. 5**) while its efficiency is increases up to $\sim 15\%$. Efficiency of $\text{SrTiO}_3(110)$ nanotubes for visible-light photocatalytical applications has been found to be much lower.

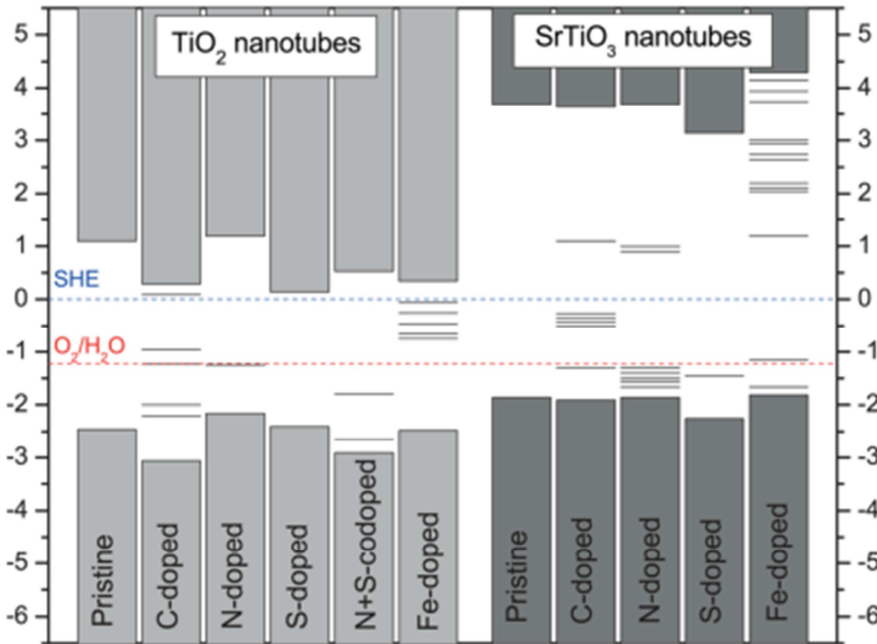


Figure 5. Schematic representation of the band edges and midgap states of periodic, pristine and doped TiO_2 and SrTiO_3 nanotubes. Blue and red horizontal dashed lines correspond to the redox potentials for H^+/H_2 and $\text{O}_2/\text{H}_2\text{O}$ dissociation, respectively. Zero of the energy scale corresponds to the standard hydrogen electrode (SHE).

The differences between the edges of band gap (VB and CB) as well as the highest occupied and lowest unoccupied impurity levels inside the band gap (HOIL and LUIL, respectively) induced in doped nanotubes must preserve the proper disposition of these levels relatively to the redox potentials, so that $\varepsilon_{\text{VB}} < \varepsilon_{\text{HOIL}} < \varepsilon_{\text{O}_2/\text{H}_2\text{O}} < \varepsilon_{\text{H}^+/\text{H}_2} < \varepsilon_{\text{LUIL}} < \varepsilon_{\text{CB}}$, thus reducing the photon energy required for dissociation of water molecule.

Energetic stability and photocatalytic activity of SrTiO₃ nanowires: *Ab initio* simulations

Yu.F. Zhukovskii

A.V. Bandura, R.A. Evarestov

Department of Quantum Chemistry, St. Petersburg State University, Russia

First principles periodic calculations based on the density functional theory within the localized atomic orbital approach (DFT-LCAO) using the hybrid exchange–correlation potential PBE0 have been performed *in close collaboration with Department of Quantum Chemistry, St. Petersburg State University (Russia)*, in order to simulate the structural and electronic properties of both stoichiometric (**Fig. 6**) and nonstoichiometric [001]-oriented four-faceted SrTiO₃ (STO) nanowires (NW) of cubic structure. Their diameters have been varied from 0.3 up to 2.4 nm with a corresponding consequent change of NW cross-section from 2×2 to 5×5 extension of the lattice constant in bulk.

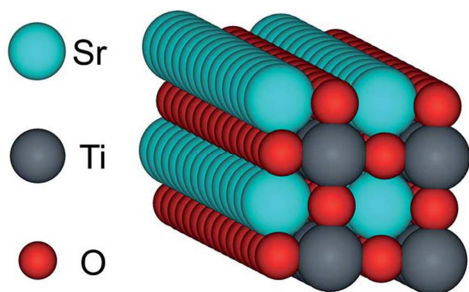


Figure 6. Axonometric image of stoichiometric [001]-oriented SrTiO₃ nanowire terminated by both SrO {100} and {010} as well as TiO₂ {100} and {010} facets with 2×2 extension of the thinnest possible 1×1 nanowire (5 atoms per UC). Left panel contains labels of constituent atoms.

Energetic stability of STO NW (both stoichiometric and non-stoichiometric) has been found to increase with the decrease of their formation energies together with the increase of NW diameter. The electronic structure calculations have shown that the width of the band gap changes in STO NWs of different structural types as compared to that in bulk being consequently reduced with the growth of NW diameter although the character of such a decrease depends on the morphology of the nanowire. Analysis of these changes shows that stoichiometric and non-stoichiometric TiO₂-terminated strontium titanate nanowires can be quite promising candidates for further applications in photocatalytic processes under solar irradiation whereas SrO-terminated NWs are rather not suitable for this purpose.

The electronic structures of mono- and bi-atomic chains of IV, III–V and II–VI group elements calculated using the DFT LCAO and LACW methods

S. Piskunov, Yu.F. Zhukovskii

P.N. D'yachkov, V.A. Zaluev

Kurnakov Institute of General and Inorganic Chemistry, Russian Academy of Sciences, Moscow, Russia

Within the current trends of miniaturization of electronic devices, the problems of interconnects between nanodevices attract growing interest in the stability, band structure, and conductivity of the nanowires. The thinnest possible nanowire is established to be a single-atom width chain. Using the first principle non-relativistic linear combination of atomic

orbitals (LCAO) and relativistic linearized augmented cylindrical wave (LACW) methods, the band structures of the covalent and partially ionic $A^N B^{8-N}$ single atom width chain have been calculated *in close collaboration with Kurnakov Institute of General and Inorganic Chemistry, Russian Academy of Sciences, Moscow*. Both methods show that the chains of C, Si, Ge, Sn, and Pb are metallic. However, there is a great difference between the relativistic and non-relativistic band structures. The π bands crossing the Fermi level are orbitally doubly degenerate in the non-relativistic model. The relativistic LACW calculations demonstrate that the spin and orbital motion of electrons are coupled, thereby splitting the π bands (**Fig. 7**).

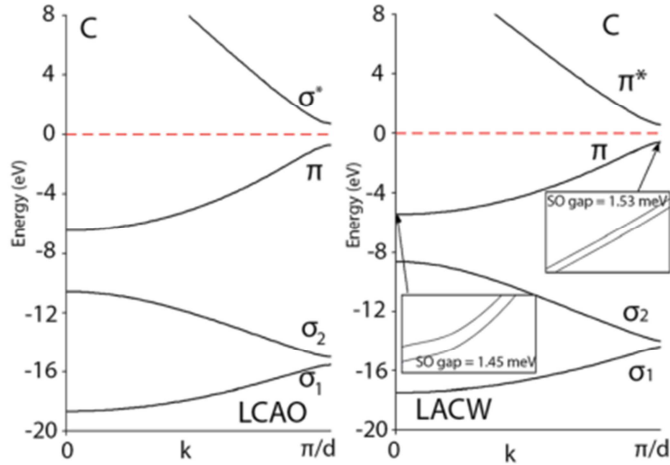


Figure 7. Non-relativistic LCAO and relativistic LACW band structures of polyyne carbene filament presented in left and right panels, respectively. Insets demonstrate splitting of the π bands.

The spin–orbit gaps are equal to 1.5 meV, 28 meV, 0.22 eV, 0.45 eV, and 4 eV for the C, Si, Ge, Sn, and Pb chains, respectively. The mass–velocity corrections result in a lowering of all the valence band levels. In the carbon and silicon chains, the corrections are possibly negligible (2–5 and 10–30 meV, respectively), while in the Ge, Sn, and Pb chains the low-energy shifts are equal to 0.6, 2.2, and 3.7 eV, respectively, due to these effects. The Darwin corrections are several times smaller in comparison to the mass–velocity contributions. The transition from the covalent chains to the partially ionic ones is accompanied by a drastic change in the band structure. The C chain with all bond lengths equal has a metal type electronic structure while the BN chain is an insulator with an energy gap equal to 6–8 eV.

The differences between the covalent and partially ionic chains are explained by the presence of the antisymmetric components of the electron potential in the latter case. The transition from the BN chain to the AIP, GaAs, and InSb ones is accompanied by a gradual decrease in the gaps; for example, the AIP chain is a semiconductor. According to the LCAO calculations, the GaAs chain is a semiconductor, but it is a metal according to the relativistic LACW method. The InSb chain possesses a metal type band structure, but the spin–orbit interaction splits the π states, forming the two π^+ and π^- sub-bands, and noticeably complicates the band structure and density of states in the vicinity of the Fermi level.

In the case of compounds from the same horizontal row in the periodic table, the transition from the $A^{III}B^V$ chains to the $A^{II}B^{VI}$ ones is accompanied by a sharp increase in the band gap. The calculations indicate the metallic nature of the InSe chain, but the CdTe one is an insulator. Among the atomic $A^N B^{8-N}$ chains, there are compounds with different electrical properties: from metals to semiconductors and insulators.

***Ab initio* simulations on Frenkel pairs of radiation defects in $\alpha\text{-Al}_2\text{O}_3$**

A. Platonenko, S. Piskunov, Yu.F. Zhukovskii, E.A. Kotomin

Corundum ($\alpha\text{-Al}_2\text{O}_3$) is important radiation-resistant material with potential applications for components of diagnostics, breeder blanket and in future fusion reactors as coating to avoid the light gases permeation. Induced changes in structural and optical properties of radiation-exposed $\alpha\text{-Al}_2\text{O}_3$ crystalline materials are mainly associated with oxygen vacancies V_O and complementary Frenkel pairs of defects (O_i+V_O). Despite technological importance of corundum crystalline structures, electronic, defects have not yet comprehensively studied theoretically. The main reasons for this are the following: the complicated atomic structure of $\alpha\text{-Al}_2\text{O}_3$ (**Fig. 8**) as well as the semi-covalent and semi-ionic chemical bonding. In this study, we have consequently performed *ab initio* calculations on (i) perfect corundum structure, (ii) that containing single point defects, such as neutral O vacancy V_O and interstitial oxygen atom O_i , (iii) that containing Frenkel pair O_i+V_O , as well as (iv) that containing dumbbell O_i+O_{reg} pair in the case of $\alpha\text{-Al}_2\text{O}_3$ structures containing either single O_i impurity or Frenkel pair.

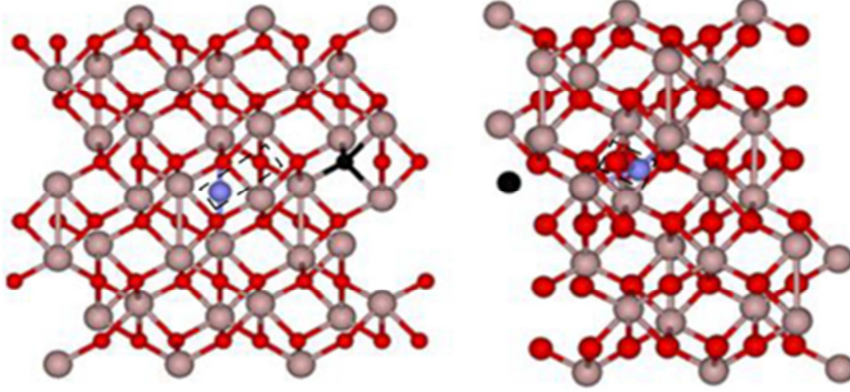


Figure 8. Images of Frenkel pair in initial and optimized corundum structures (left and right panels, respectively). V_O vacancy is shown as a black ball while the interstitial O_i atom is shown as a blue (dark grey) one. Configurations of dumbbell are shown as a dotted rectangle.

Using optimization procedure, we have determined equilibrium locations and configurations of V_O , O_i , and O_i+V_O inside corundum lattice. After relaxation of the ideal supercell structure, the optimized $d_{O_i-V_O}$ distance has been found to be ~ 4.5 Å while the formation energy of Frenkel pair has achieved 11.7 eV. The interstitial O_i atom, both single and a component of O_i+V_O pair, spontaneously forms a dumbbell with the adjacent atom in the regular oxygen sublattice ($d_{O_i-V_O} = 1.404$ Å) with the induced charge $-1.1 e$. On the whole, possibilities of supercell model for proper description of Frenkel pairs with changing inter-defect distance and space orientation inside corundum crystal are rather limited. In order to simulate well-separated Frenkel pairs of varying length as well as charged and excited defects, a cluster model will be used in the next studies, which also excludes artifacts caused by the periodic network of defect-defect interactions.

First principles hybrid DFT calculations of $\text{BaTiO}_3/\text{SrTiO}_3$ (001) interface

S. Piskunov and R.I. Eglitis

We performed *ab initio* calculations for $\text{BaTiO}_3/\text{SrTiO}_3$ (001) interfaces taking into account non-stoichiometric compositions. Using B3PW hybrid exchange-correlation functional inside the density functional theory (DFT) we demonstrate that charge

redistribution in the interface region weakly affects the electronic structure of the studied material (**Fig. 9**).

The key effect found at BaTiO₃/SrTiO₃ (001) interfaces is strong dependence of the band gap on the external BaO or TiO₂ (001) termination. This effect is much stronger, than the dependence of the interface band gap on the number of augmented layers upon the substrate.

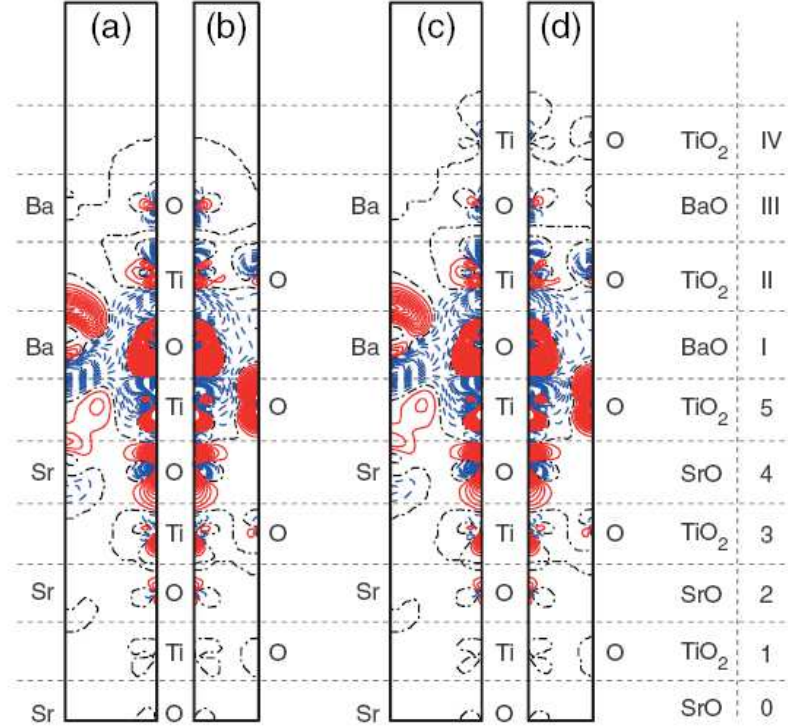


Figure 9. Difference electron charge density maps calculated for BTO/STO (001) heterostructures: (a) (110) cross-section for $N_{\text{BTO}} = 3$, (b) (100) cross-section for $N_{\text{BTO}} = 3$, (c) (110) cross-section for $N_{\text{BTO}} = 4$, (d) (100) cross-section for $N_{\text{BTO}} = 4$. Red solid (dark gray), blue dashed (light gray) and black dashed-dot isolines describe positive, negative and zero values of the difference charge density, respectively. Isodensity curves are drawn from -0.025 to $+0.025 e \text{ \AA}^{-3}$ with an increment of $0.0005 e \text{ \AA}^{-3}$. Right-side bar shows the atomic monolayers from which atoms are originated. STO and BTO monolayers are numbered beginning from the center of slab (0 means the central monolayer of the symmetrical slab unit cell). Monolayers are numbered separately for STO (001) substrate and for BTO (001) nanofilm using Arabic and Roman numbers.

From determination of the fugacity coefficients to estimate of hydrogen storage capacity: A convenient theoretical method

R. I. Eglitis

P. Fu, R. Jia, C.-P. Kong, , H.-X. Zhang
Beijing Institute of Technology, Beijing, China

The equation of state (EOS) from virial expansion (VE) was used to pave the way for determining the fugacity coefficients of the hydrogen fluid at arbitrary temperature and pressure. The fugacity coefficients from our VE method have more physical meaning than the empirical values. In this way, the hydrogen storage capacity of a novel material model have

been estimated *in a close collaboration with Beijing Institute of Technology, China*, using a few density functional theory (DFT) calculations with the aid of a continuum model.

The efficient continuum model can provide a more accurate estimation of the hydrogen storage capacity than the direct DFT calculations. Furthermore, the expensive grand canonical ensemble (μ_{NT}) simulations combining with the quantum mechanics methods (*i.e.*, QM/MD- μ_{NT}) are unnecessary within this method. The hydrogen fluid can be handled with our VE method at the temperature in the range of 160-773 K. The hydrogen storage capacity and the detailed thermodynamic information of a designed novel material can thereby be estimated using this method with relatively high accuracy and low computing cost. As an example, the hydrogen storage capacities of the expanded bilayer graphene systems were calculated. Our theoretical results are in an excellent agreement with experimental results.

CNTs- and GNRs-based electromagnetic and spintronic devices: Models and simulations

Yu.N. Shunin, Yu.F. Zhukovskii

V.I. Gopeyenko, N.Yu. Burlutskaya

Natural Sciences and Computer Technologies Department, Information Systems Management Institute, ISMA University, 1 Lomonosov Str., Bld 6, LV-1019, Riga, Latvia

T.D. Lobanova-Shunina

Technical University, Institute of Aeronautics 1 Lomonosov Str., Bld V, LV-1019, Riga, Latvia

S. Bellucci

Laboratori Nazionali di Frascati, Via Enrico Fermi 40, Frascati, Italy

Fundamental electromagnetic and electromechanical properties of CNTs, graphene nanoribbons (GNR) and nanofibers (GNF), CNT- and graphene-based aerogels (CNTBA, GBA), CNT- and graphene-based 3D-nanofoams and carbon-based polymer nanocomposites are essential for various nanotechnology applications, *e.g.*, for engineering new classes of ultra-light, highly conductive nanomaterials with exceptional mechanical strength, flexibility, and elasticity. These nanomaterials are the basis for unique nanoelectronic devices and nanosensors. Particular properties of carbon-based nanoporous systems in dependence on porosity extent, morphology and fractal dimension allow finding practically useful correlations between their mechanical and electrical properties. Electromagnetic properties of CNTs and GNRs nanostructures with functionalized atomic groups and their various interconnects with the essential concentration of ‘dangling bonds’ are very sensitive to local external perturbations. The induced changes of local electronic density of states lead to the correlated changes of current and spin states. Models of nanocarbon spintronic devices are developed as memory nanodevices, particularly, based on magneto-resistance phenomena. Models of nanocomposite carbon-based materials and nanodevices are proposed (**Fig. 10**).

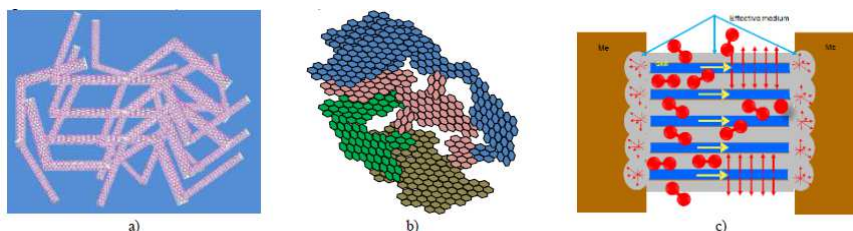


Figure 10. A set of models: a) structural model of CNTBA; b) model of GBA; c) GNRs-based gas nanosensor device.

The main objective of the current study is to demonstrate the implementation of advanced simulation models to ensure a proper description of the electronic properties, electrical conductivity, electromagnetic and electromechanical phenomena of functionalized CNT- and GNR-based nanostructures of different morphologies and their interconnects for nanosensor and nanomemory systems. The sensitivity of the local electronic density of states to external influences (mechanical, chemical, magnetic, *etc.*) on the fundamental electromagnetic properties of CNTs, GNRs and their metal interconnects are analyzed from the point of view of nanosensor applications. We develop prospective models of nanocarbon-based nanomaterials and nanodevices which are based on various interconnects and interfaces.

B. Kinetics of processes with self-organization

Effects of pressure, temperature and atomic exchanges on phase separation dynamics in Au/Ni(111) surface alloy: Kinetic Monte Carlo study

G. Zvejnieks

A. Ibenskas, E.E. Tornau

Center for Physical Sciences and Technology, Semiconductor Physics Institute, Vilnius, Lithuania

Instability of the Au/Ni(111) surface alloy has been studied under different CO gas pressure, p , and temperature limits, using the kinetic Monte Carlo simulations. We have analyzed the reaction front dynamics and formation of Au clusters, using the model which takes into account surface adatom pair- and three-body interactions, CO adsorption and desorption, catalytic carbonyl formation reaction, Au and Ni adatom diffusion and their concerted exchange. Variation of interaction parameters has allowed us to identify three possible reaction front propagation limits with different pressure dependencies (**Fig. 11**):

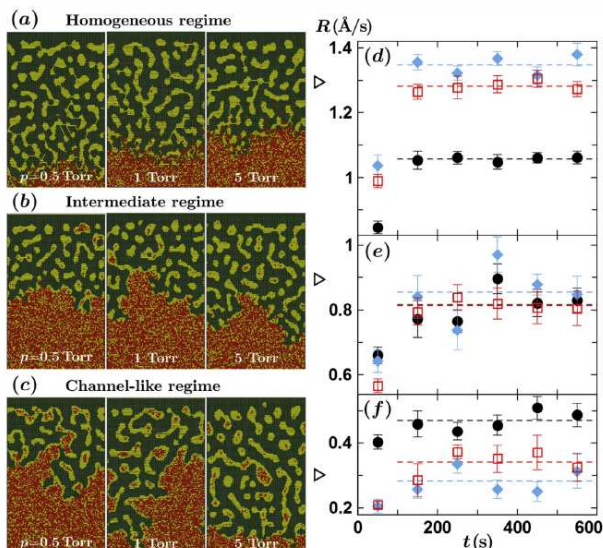


Figure 11. Lattice snapshots (90×40) at different pressures of CO gas and corresponding step-flow rates.

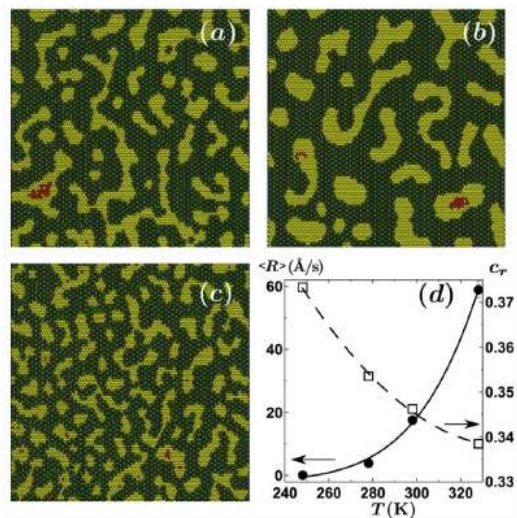


Figure 12. Lattice fragments (100×100) of Au islands at: (a) $T=248$ K, (b) $T=328$ K, (d) average SFR (solid line) dependence on temperature.

(i) slow channel-like flow in agreement with experimental data (Step Flow Rate – SFR, R , increases with p), (ii) intermediate regime (weak dependence), and (iii) fast homogeneous flow (R decreases with p).

We have found that only Au-Ni exchange, contrary to both Ni-CO and Au-CO exchanges, significantly reduces the number of screened Ni atoms inside the Au clusters and stimulates the occurrence of Ni-free Au clusters. The size of Au islands depends on both pressure and temperature. At a fixed temperature it decreases with pressure due to an increased SFR. In the high temperature limit, despite the SFR exponential increase with temperature, the cluster size increases due to an enhanced Au mobility (**Fig. 12**).

On canonical quantization of electron-hole acoustic phonon crystalline systems

E. Klotins

Methods of quantum electrodynamics are elaborated with application to consistent relativistic theory of open quantum systems. The study is motivated by developments of light-matter interaction which has excited interest in the description of important quantum systems for which interactions between the charged particles play a major role.

Special attention is paid to dielectrics and their interaction with electromagnetic (optical) radiation. The physical model includes spatially periodic structure of atoms supporting quasiparticles categorized as electrons, holes and acoustic phonons each having a complex influence on its neighbors and represents a challenge for extensively developing theory of condensed state. Particular problems are addressed to birth and annihilation of these quasi-particles, interacting both with the radiation and the acoustic oscillations of the ionic subsystem (phonons).

Obtained results include transition from the macroscopic description to the quantum kinetics for the constituting quasi-particles in a unified framework of nonstationary and nonequilibrium distribution functions. Rationale of these results is clues to dynamic effects induced by femto-second light pulses and the relaxation of quasiparticles. Extensions that embody more complex models and higher order energy derivatives are available as advancement.

C. Plasma Physics

Non-stationary oscillations in gyrotrons revisited

O. Dumbrajs

H. Kalis

Institute of Mathematics and Computer Science, University of Latvia, Riga, Latvia

Development of gyrotrons requires detailed understanding of different regimes of gyrotron oscillations. It is known that in the planes of the generalized gyrotron variables: cyclotron resonance mismatch and dimensionless current or cyclotron resonance mismatch

and dimensionless interaction length complicated alternating sequences of regions of stationary, periodic, auto modulation, and chaotic oscillations exist. In the past, these regions were investigated on the supposition that the transit time of electrons through the interaction space is much shorter than the cavity decay time. This assumption is valid for short and/or high diffraction quality resonators. However, in the case of long and/or low diffraction quality resonators, which are often utilized, this assumption is no longer valid. In such a case a different mathematical formalism has to be used for studying nonstationary oscillations. One example of such formalism has been described in our paper (**Fig. 13**).

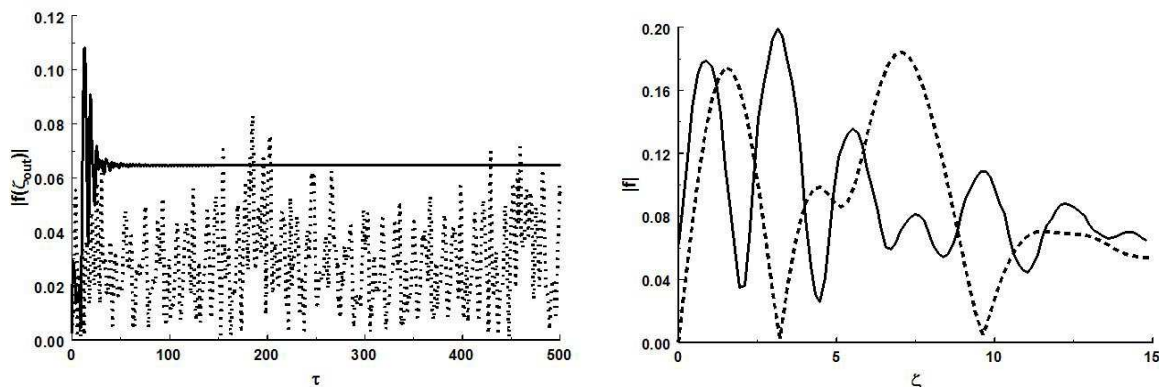


Figure 13. Left: rf field amplitude at the resonator end as a function of time. Right: the field profile in the cavity. The solid curves were obtained when $t_{decay} \gg t_{transit}$ ($t_{decay} \sim Q/\omega$, $t_{transit} = L/v_z$, Q is the quality factor, ω is the oscillation frequency, L is the interaction length, and v_z is the longitudinal velocity). (1) and (2) and the dashed curves when $t_{decay} \approx t_{transit}$.

Field formation in the interaction space of gyrotrons

O. Dumbrajs,

G.S. Nusinovich

Institute for Research in Electronics and Applied Physics, University of Maryland, College Park, USA

For gyrotron applications in plasma installations, one of the most important factors is the gyrotron efficiency. To maximize the interaction efficiency, it is necessary not only to optimize such operating parameters as the magnetic field, beam voltage and current, but also the axial profile of the electromagnetic (EM) field in the interaction space.

In collaboration with Institute for Research in Electronics and Applied Physics, University of Maryland, we have performed a study of the effect of the profile of an irregular waveguide serving as a resonator on the axial structure of the EM field. Specific attention has been paid to the profile of the uptaper connecting the regular part of a resonator to the output waveguide (**Fig. 14**). Conditions of applicability of the nonuniform string equation, which is widely used in gyrotron designs for finding the axial structure of the EM field, were also discussed, as well as the occurrence of reflections from a smooth uptaper and the analogy between the nonuniform string equation and the stationary Schrödinger equation.

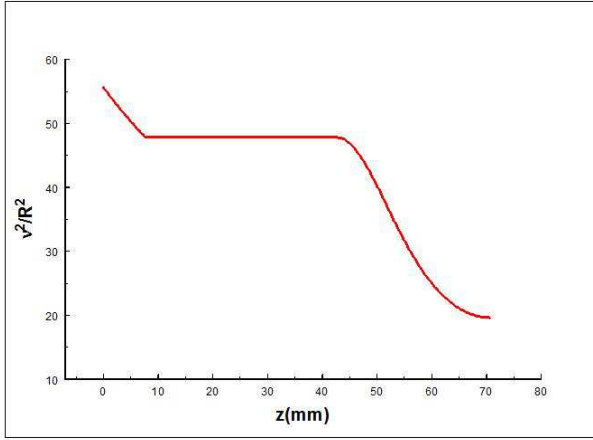


Figure 14. The well of the gyrotron potential in contrast to ordinary quantum mechanics potentials has no wall on the right hand side.

Bifurcations and fast-slow dynamics in a low-dimensional model for quasi-periodic plasma perturbations

O. Dumbrajs

D. Constantinescu, V. Igochine, K. Lackner, H. Zohm

Max-Planck Institut für Plasmaphysik, Association Euratom-IPP, Garching, Germany

Oscillations of plasma's parameters (saw teeth, edge localized modes, frequently interrupted regime of neoclassical tearing modes) are observed when some large scale plasma instabilities do not lead to an immediate termination of a discharge. The understanding of such phenomena is an important tool in controlling the whole reaction. There are many fundamental approaches to the subject, but, despite the huge theoretical and experimental efforts, these phenomena are not fully understood. We have focused on a low dimensional model which describes the dynamics of the plasma pressure gradient and of the amplitude of the magnetic field displacement.

Our low-dimensional model is given by

$$\begin{cases} \frac{d^2}{dt^2} \zeta = (p' - 1) \cdot \zeta - \delta \cdot \frac{d}{dt} \zeta \\ \frac{d}{dt} p' = \eta \cdot (h - p' - \zeta^2 \cdot p') \end{cases}$$

where ζ is the amplitude of the magnetic field displacement, p' is the plasma pressure gradient at the plasma edge, t is time, δ is dissipation/relaxation of the instability responsible for the ELM burst, η is diffusion and h is input power in the system. The first equation describes the evolution of the magnetic field perturbation and relaxation dynamics. The second equation describes power balance in the system including the effect of unstable modes.

This system is important both from a mathematical and a practical point of view. It was introduced in order to explain the quasiperiodic plasma dynamics observed in fusion experiments in Tokamaks. The system has some similar properties with the Lorenz system (dissipativity and symmetry). It is a fast-slow system. We have analyzed the stability of the equilibrium points studying some bifurcations of the system (pitchfork and Hopf bifurcations).

D. Experimental Studies

Excitation spectra of the emissions at 1.6 eV and 1.42 eV in MgO:Cr single crystals

A.I. Popov

E. Shablonin, A. Lushchik, S. Dolgov
Institute of Physics, University of Tartu, Estonia

A. Kotlov

Deutsches Elektronen-Synchrotron DESY, Notkestraße 85, 22607 Hamburg, Germany

Role of impurities, especially at their high concentrations, in the processes of the relaxation of the electronic excitation is still hot topic in radiation solid state physics. The excitation spectra for the emission of chromium-containing centres have been measured at 10 K using synchrotron radiation of 4–32 eV in MgO single crystals with different content of Cr^{3+} (5 to 850 ppm) and Ca^{2+} impurity ions. Both virgin crystals and the samples preliminarily irradiated with x-rays at 295 K have been studied.

Some typical spectra measured at DESY-synchrotron radiation facility are shown in **Fig. 15**

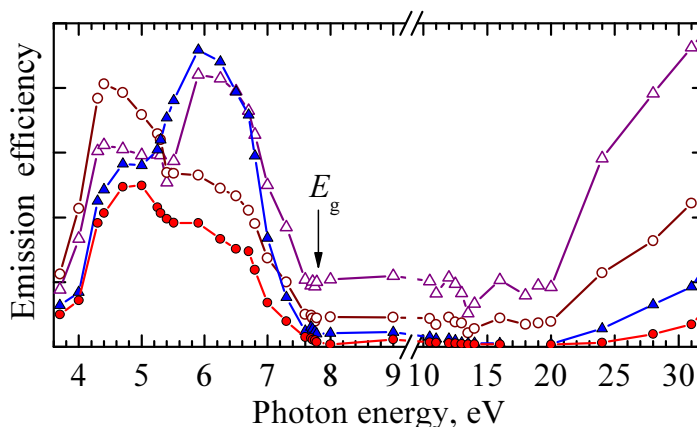


Figure 15. Excitation spectra of the emissions at 1.6 eV (\blacktriangle , \triangle) and 1.42 eV (\bullet , \circ) measured at 10 K for virgin (\blacktriangle , \bullet) and x-irradiated (\triangle , \circ) MgO:Cr (850 ppm) crystals

The role of complex chromium centres containing two Cr^{3+} cations and a vacancy (sometimes nearby a Ca^{2+} ion) in the luminescence processes and the transformation/creation of structural defects has been analysed. According to **Fig. 15**, the influence of preliminary X-irradiation on the excitation spectra for the emissions at 1.42 or 1.6 eV related to pair chromium centres at $h\nu > E_g$ is nearly the same as for R- and N-emission. However, below 7 eV the spectra difference for virgin and x-irradiated samples of MgO:Cr (850 ppm) is more complicated. It is worth noting that even a prolonged irradiation with $h\nu \sim 20$ eV at 10 K causes the recharging of some Cr^{3+} into Cr^{2+} . The intensity of Cr^{3+} -emission considerably decreases with a crystal cooling from 77 to 10 K. In our opinion, the effect is caused by the attenuation of the emission related to ^{54}Cr isotope with nuclear spin $I = 0$, while MgO:Cr (850 ppm) contains also ~ 80 ppm of ^{53}Cr ($I = 3/2$) ions the emission of which can be observed at 10 K.

FTIR studies of silicon carbide 1D-nanostructures

A. I. Popov,

I. Karbovnyk, P. Savchyn

Ivan Franko National University of Lviv, Ukraine

A Huczko,

Department of Chemistry, Warsaw University, Poland

M Cestelli Guidi,

INFN-Laboratori Nazionali di Frascati, Italy

Stable 1D silicon carbide (SiC) nanostructures have been prepared *via* combustion synthesis route which is widely used for the fabrication of various nanomaterials. The examination of the raw reaction product (in the form of a powder) has shown that it actually consists of a mixture of SiC nanowires, distributed in diameter range from tens of nanometers to 100 nm, C nanocrystallites and remaining Si. In order to obtain pure SiC nanowires, wet-chemistry three-stage protocol was used. Structural studies have indicated that the obtained modification of SiC is 3C polytype with a cubic unit cell. The IR spectroscopy has been performed at SINBAD infrared beamline of Daphne Light synchrotron facility. IR absorption and reflection spectra for as-obtained and purified SiC nanowires have been compared with the spectra of commercially available SiC nanomaterials (**Figs. 16, 17**). Principal vibrational modes have been identified. Reflectivity spectrum has been reconstructed by modelling of the dielectric function (**Figs. 18, 19**).

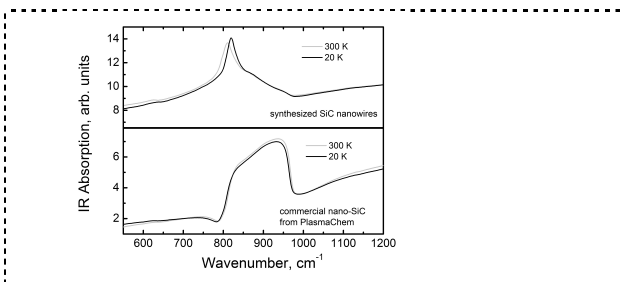


Figure 16. IR absorption spectra of SiC nanowires (upper part) as compared to the IR spectra of commercial SiC nanopowder.

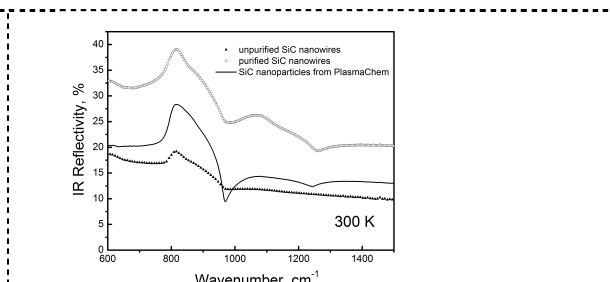


Figure 17. IR reflectivity of purified/unpurified SiC nanowires and commercial SiC nanopowder at 300 K.

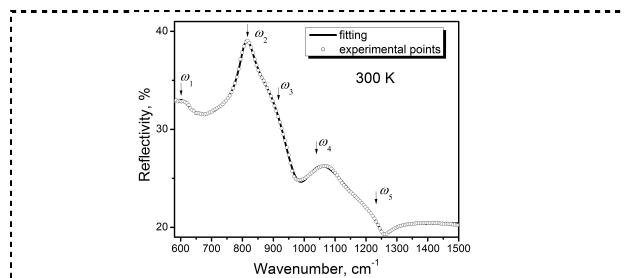


Figure 18. Experimental and calculated IR reflectivity of SiC nanowires. Arrows indicate the identified vibrational modes.

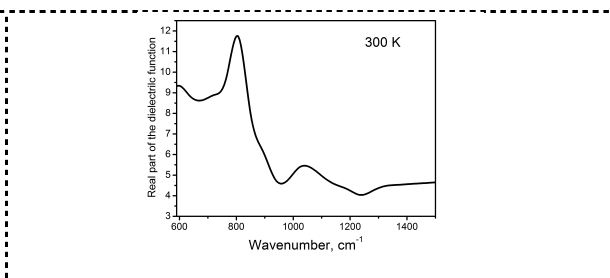


Figure 19. Real part of the dielectric function calculated for SiC nanowires in the frame of the factorized model.

The obtained frequencies of main vibrational modes of SiC nanowires are summarized in Table 1.

$\omega_{1\text{TO}}$, cm^{-1}	$\omega_{1\text{LO}}$, cm^{-1}	$\omega_{2\text{TO}}$, cm^{-1}	$\omega_{2\text{LO}}$, cm^{-1}	$\omega_{3\text{TO}}$, cm^{-1}	$\omega_{3\text{LO}}$, cm^{-1}	$\omega_{4\text{TO}}$, cm^{-1}	$\omega_{4\text{LO}}$, cm^{-1}	$\omega_{5\text{TO}}$, cm^{-1}	$\omega_{5\text{LO}}$, cm^{-1}
596	596	812	813	917	975	1018	1082	1258	1258

Obtained results show clear effect of nanostructure's morphology on the both IR absorption and reflectivity. In particular, vibrational modes, mostly depending on the morphology, were detected.

Defences of M.Sc. Theses

1. **A. Česnokovs**, TiO₂ nanocauruļu fotokatalītiskās aktivitātes kvantu ķīmijas pētījums. Maģistra darba disertācija. Latvijas Universitāte (Ķīmijas fakultāte, Rīga, 2015. g. jūnijā).
2. **O. Lisovski**, DFT modeling of S and N co-doped anatase (101) TiO₂ nanotubular photocatalysts for water splitting. Master Thesis. Uppsala University (Master Program in Chemistry, Uppsala, 2015, June).

Defence of B.Sc. Thesis

3. **M. Sokolovs**, ODS nanodaļiņu veidošanās *bcc*-Fe tilpumā sākuma stadiju modelēšana no pirmajiem principiem. Bakalaura darba disertācija. Latvijas Universitāte. (Fizikas un matemātikas fakultāte, Rīga, 2015. g. jūnijā).
-

Publications in 2015

SCI

1. E. Heifets, **E.A. Kotomin**, A.A. Bagaturyants, and J. Maier, Ab initio study of BiFeO₃: Thermodynamic stability conditions. - *J. Phys. Chem. Lett.*, 2015, 6, p. 2847–2851. Impact Factor (IF): **7.46**
2. T.S. Bjørheim, **E.A. Kotomin**, and J. Maier, Hydration entropy of BaZrO₃ from first principles phonon calculations. - *J. Mater. Chem. A*, 2015, 3, p. 7639–7648. **IF: 7.44**
3. **S. Piskunov**, **O. Lisovski**, J. Begens, **D. Bocharov**, **Yu.F. Zhukovskii**, M. Wessel, and E. Spohr, C-, N-, S-, and Fe-doped TiO₂ and SrTiO₃ nanotubes for visible-light-driven photocatalytic water splitting: Prediction from first principles. - *J. Phys. Chem. C*, 2015, 119, p. 18686–18696. **IF: 4.77**
4. T.S. Bjørheim, M. Arrigoni, **D. Gryaznov**, **E.A. Kotomin**, and J. Maier, Thermodynamic properties of neutral and charged oxygen vacancies in BaZrO₃ based on first principles phonon calculations. - *Phys. Chem. Chem. Phys.*, 2015, 17, p. 20765–20774. **IF: 4.49**
5. A.V. Bandura, R.A. Evarestov, and **Yu.F. Zhukovskii**, Energetic stability and photocatalytic activity of SrTiO₃ nanowires: Ab initio simulations. - *Royal Soc. Chem. Advances*, 2015, 5, p. 24115–24125. **IF: 3.84**

6. P.N. D'yachkov, V.A. Zaluev, **S. Piskunov**, and **Yu.F. Zhukovskii**, Comparative analysis of the electronic structures of mono- and bi-atomic chains of IV, III–V and II–V group elements calculated using the DFT LCAO and LACW methods. - *Royal Soc. Chem. Advances*, 2015, 5, p. 91751–91759. **IF: 3.84**
7. P. Fu, R. Jia, C.-P. Kong, **R.I. Eglitis**, and H.-X. Zhang, From determination of the fugacity coefficients to estimation of hydrogen storage capacity: A convenient theoretical method. - *Int. J. Hydrogen Energ.*, 2015, 40, p. 10908-10917. **IF: 3.31**
8. **G. Zvejnieks**, A. Ibenskas, and E.E. Tornau, Effects of pressure, temperature and atomic exchanges on phase separation dynamics in Au/Ni(111) surface alloy: Kinetic Monte Carlo study. - *J Alloy Compd.*, 2015, 649, p. 313-319. **IF: 3.00**
9. **R.I. Eglitis**, Ab initio hybrid DFT calculations of BaTiO₃, PbTiO₃, SrZrO₃ and PbZrO₃ (111) surfaces. - *Appl. Surf. Sci.*, 358, 2015, p. 556-562. **IF: 2.71**
10. A.U. Abuova, **Yu.A. Mastrikov**, **E.A. Kotomin**, Y. Kawazoe, T.M. Inerbaev, and A.T. Akilbekov, First principles modeling of Ag adsorption on the LaMnO₃ (001) surfaces. - *Solid State Ionics*, 2015, 273, p. 46–50. **IF: 2.56**
11. S. Piskunov and R.I. Eglitis, First principles hybrid DFT calculations of BaTiO₃/SrTiO₃ (001) interface. - *Solid State Ionics*, 2015, 274, p. 29-33. **IF: 2.56**
12. G.A. Kaptagay, T.M. Inerbaev, **Yu.A. Mastrikov**, **E.A. Kotomin**, and A.T. Akilbekov, Water interaction with perfect and fluorine-doped Co₃O₄ (100) surface. - *Solid State Ionics*, 2015, 277, p. 77–82. **IF: 2.56**
13. **O. Dumbrajs** and H. Kalis, Nonstationary oscillations in gyrotrons revisited. - *Phys. Plasmas*, 2015, 22, 053113 (p. 1-6). **IF: 2.14**
14. G.S. Nusinovich and **O. Dumbrajs**, Field formation in the interaction space of gyrotrons. - *J. Infrared Milli. Terahz. Waves*, 2015, 36, p. 1-12. **IF: 1.94**
15. T. Idehara, E.M. Khutoryan, Y. Tatematsu, Y. Yamaguchi, A.N. Kuleshov, **O. Dumbrajs**, Y. Matsuki, and T. Fujiwara, High-speed frequency modulation of a 460-GHz gyrotron for enhancement of 700-MHz DNP-NMR spectroscopy. - *J. Infrared Milli. Terahz. Waves*, 2015, 36, p. 819-829. **IF: 1.94**
16. D. Constantinescu, **O. Dumbrajs**, V. Igochine, K. Lackner, H. Zohm and ASDEX Upgrade team, Bifurcations and fast-slow dynamics in a low-dimensional model for quasi-periodic plasma perturbations. - *Romanian Reports Phys.*, 2015, 67, p. 1049–1060. **IF: 1.52**
17. M. Arrigoni, **E.A. Kotomin**, **D. Gryaznov**, and J. Maier, Confinement effects for the F center in non-stoichiometric BaZrO₃ ultrathin films. - *Phys. Status Solidi B*, 2015, 252, p. 139–143. **IF: 1.49**
18. **R.I. Eglitis**, Comparative *ab initio* calculations of SrTiO₃ and CaTiO₃ polar (111) surfaces. - *Phys. Status Solidi B*, 2015, 252, p. 635–642. **IF: 1.49**
19. J.R. Kalnin and **E.A. Kotomin**, The effective diffusion coefficient in a one-dimensional discrete lattice with the inclusions. - *Physica B*, 2015, 470-471, p. 50–52. **IF: 1.32**

20. E. Shablonin, **A.I. Popov**, A. Lushchik, A. Kotlov, and S. Dolgov, Excitation of different chromium centres by synchrotron radiation in MgO:Cr single crystals. - *Physica B*, 2015, 477, p. 133-136. **IF: 1.32**
21. **R.I. Eglitis**, Theoretical prediction of the 5V rechargeable Li ion battery using $\text{Li}_2\text{CoMn}_3\text{O}_8$ as a cathode. - *Phys. Scr.*, 2015, 90, 094012 (p.1-4) **IF: 1.13**
22. **A. Chesnokov**, **O. Lisovski**, **D. Bocharov**, **S. Piskunov**, **Yu.F. Zhukovskii**, M. Wessel, and E. Spohr, Ab initio simulations on N and S co-doped titania nanotubes for photocatalytic applications. - *Phys. Scr.*, 2015, 90, 094013 (p.1-7). **IF: 1.13**
23. A.V. Bystrova, Y.D. Dekhtyar, **A.I. Popov**, J. Coutinho, and V.S. Bystrov, Modified hydroxyapatite structure and properties: Modeling and synchrotron data analysis of modified hydroxyapatite structure. - *Ferroelectrics*, 2015, 475, p. 135-147. **IF: 0.47**
24. **R.I. Eglitis**, Comparative first-principles calculations of SrTiO_3 , BaTiO_3 , PbTiO_3 and CaTiO_3 (001), (011) and (111) surfaces. - *Ferroelectrics*, 2015, 483, p. 53-67. **IF: 0.47**
25. **R.I. Eglitis**, Theoretical modelling of the energy surface (001) and topology of CaZrO_3 perovskite. - *Ferroelectrics*, 2015, 483, p. 75-85. **IF: 0.47**
26. A. Anspoks, J. Timoshenko, **D. Bocharov**, J. Purans, F. Rocca, A. Sarakovskis, V. Trepakov, A. Dejneka, and M. Itoh, Local structure studies of Ti for $\text{SrTi}^{16}\text{O}_3$ and $\text{SrTi}^{18}\text{O}_3$ by advanced X-ray absorption spectroscopy data analysis. - *Ferroelectrics*, 485, 2015, p. 42–52. **IF: 0.47**
27. **A. Platonenko**, **S. Piskunov**, **Yu.F. Zhukovskii**, and **E.A. Kotomin**, Ab initio simulations on Frenkel pairs of radiation defects in corundum. - *IOP Conf. Ser. Mater. Sci. Eng.*, 2015, 77, 012001 (pp. 1-5).
28. **E. Klotins**, On time-resolved approach for phonon assisted interband transitions. - *IOP Conf. Ser. Mater. Sci. Eng.*, 2015, 77, 012003 (pp. 1-9).
29. I. Karbovnyk, P. Savchyn, A. Huczko, M. Cestelli Guidi, C. Mirri, and **A.I. Popov**, FTIR studies of silicon carbide 1D-nanostructures. - *Materials Science Forum*, 2015, 821-823, p. 261-264.

Chapters in Scientific Books

1. **Yu.N. Shunin**, Spintronic Nanomemory and Nanosensor Devices (Lambert Academic Publishing, Saarbrücken), 2015, p. 2-49.

Non-SCI papers

1. S. Bellucci, F. Micciulla, **Yu.N. Shunin**, **Yu.F. Zhukovskii**, V.I. Gopeyenko, N. Burlutskaya, T. Lobanova-Shunina, and A. Capobianchi, Memory nanodevices based on carbon nanotube-Fe-Pt interconnects: Electromagnetic simulations and magnetically stimulated nanotube growth. - *J. Mater. Sci. Eng. B*, 2015, 5, p. 120-134.
2. **Yu.N. Shunin**, **Yu.F. Zhukovskii**, V.I. Gopeyenko, N. Burlutskaya, T. Lobanova-Shunina, and S. Bellucci, CNTs- and GNRs-based electromagnetic and spintronic devices: Models and simulations. - *Proc. Internat. Conf. „Physics, Chemistry and Application of*

- Nanostructures (Nanomeeting-2015, Minsk, Belarus)*” (Eds. V.E. Borisenko, S.V. Gaponenko, V.S. Gurin, and C.H. Kam; World Scientific, New Jersey, London, Singapore, Beijing, Shanghai, Hong Kong, Taipei, Chennai), 2015, p. 207-210.
3. **Yu.N. Shunin**, S. Bellucci, **Yu.F. Zhukovskii**, V.I. Gopeyenko, N. Burlutskaya, and T. Lobanova-Shunina, Nanocarbon electromagnetics in CNT-, GNR- and aerogel-based nanodevices: models and simulations. - *Computer Modelling & New Technologies*, 2015, 19(1A), p. 35-42.
 4. **Yu.N. Shunin**, S. Bellucci, **Yu.F. Zhukovskii**, T. Lobanova-Shunina, N. Burlutskaya, and V.I. Gopeyenko, Modelling and simulation of CNTs- and GNRs-based nanocomposites for nanosensor devices. - *Computer Modelling & New Technologies*, 2015, 19(5A), p. 14-20.
 5. D. Fink, A. Kiv, **Yu.N. Shunin**, N. Mykytenko, T. Lobanova-Shunina, A. Mansharipova, T. Koycheva, R. Muhamediev, V. Gopeyenko, N. Burlutskaya, **Yu.F. Zhukovskii**, and S. Bellucci, The nature of oscillations of ion currents in the ion track electronics. - *Computer Modelling & New Technologies*, 2015, 19(6), p. 7-13.
-

Presentations at Scientific Conferences, Meetings, and Workshops in 2015

I. 31th ISSP Conference (Riga, Latvia, February, 2015).

1. **O. Dumbrajs**, “Applications of gyrotrons for studies of particles in nuclear and solid state physics”. Abstract: p. 21.
2. **A. Platonenko**, **S. Piskunov**, **Yu.F. Zhukovskii**, and **E.A. Kotomin**, “Ab initio simulations on neutral point defects and Frenkel pairs in corundum”. Abstract: p. 40.
3. **A. Gopejenko**, **Yu.F. Zhukovskii**, **P.V. Vladimirov**, **E.A. Kotomin**, **Yu.A. Mastrikov**, **V.A. Borodin**, and **A. Möslang**, “Ab initio calculations of Y, O and V_{Fe} diffusion barriers inside fcc-Fe lattice”. Abstract: p. 41.
4. **A. Chesnokov**, **O. Lisovski**, **D. Bocharov**, **S. Piskunov**, and **Yu.F. Zhukovskii**, “Connection between electronic structure of TiO_2 nanotubes and their morphology: Ab initio study”. Abstract: p. 42.
5. **M. Sokolov**, **Yu.A. Mastrikov**, and **E.A. Kotomin**, “Optimization of the electron charge density integration parameters using the Bader method”. Abstract: p. 74.

II. 9th International Conference on Materials Science & Engineering, BRAMAT2015 (Brasov, Romania, March, 2015).

6. **R. I. Eglitis**, “Towards a practical rechargeable 5 Volt Li ion battery using $Li_2CoMn_3O_8$ as a battery cathode material”. Abstract: p. 24.
7. **R. I. Eglitis**, “Ab initio calculations of $SrTiO_3$, $BaTiO_3$, $PbTiO_3$ and $CaTiO_3$ perovskite (001), (011) and (111) surfaces”. Abstract: p. 25.
8. **R.I. Eglitis**, **H. Shi**, and **R. Jia**, “Large scale ab initio calculations of the diffusion and aggregation of F centers, as well as bulk and nano-surface H centers in CaF_2 , BaF_2 and SrF_2 ”. Abstract: p. 282.

III. 49th Russian School on Condensed State Physics (St. Petersburg, Russia, March, 2015).

9. **A. Platonenko**, **S. Piskunov**, **Yu.F. Zhukovskii**, and **E.A. Kotomin**, “Ab initio simulation of point defects and Frenkel pairs in corundum crystal”. Abstract: p. 168.

IV. 4th International Conference "Multifunctional, Hybrid and Nanomaterials (Barcelona, Spain, March, 2015).

10. **A.I. Popov**, V.P. Savchyn, **A. Moskina**, E. Elsts, and **R.I. Eglitis**, "Comparative studies of cathodoluminescence properties of BaZrO₃, SrTiO₃ and KBr crystals". Abstract: P3.289.

V. PSI Nuclear Materials Workshop (Meiringen, Switzerland, March, 2015).

11. **D. Bocharov**, M. Chollet, M. Krack, J. Bertsch, D. Grolimund, M. Martin, A. Kuzmin, J. Purans, and **E.A. Kotomin**, "Simulation of chromia-doped uranium dioxide".

VI. 13th International Conference "Information Technologies and Management", IT&M'2015 (Riga, Latvia, April, 2015).

12. **Yu.N. Shunin**, D. Fink, S. Bellucci, A.E. Kiv, T. Lobanova-Shunina, **Yu.F. Zhukovskii**, and V.I. Gopeyenko, "Nanotechnology and health nanodiagnostic tools". Abstract: p. 15-17.

13. **Yu.N. Shunin**, S. Bellucci, T. Lobanova-Shunina, **Yu.F. Zhukovskii**, N. Burlutskaya, and V.I. Gopeyenko, "Models and simulations of CNTs- and GNRs-based electromagnetic and spintronic devices". Abstract: p. 18-20.

14. **A. Gopejenko**, **Yu.F. Zhukovskii**, P.V. Vladimirov, V.A. Borodin, **E.A. Kotomin**, **Yu.A. Mastrikov**, and A. Möslang, "Ab initio calculations of Y, O and V_{Fe} migration barriers inside fcc-Fe lattice". Abstract: p. 21.

15. **Yu.F. Zhukovskii**, R.A. Evarestov, and A.V. Bandura, "Photocatalytic efficiency of SrTiO₃ nanowires: ab initio modeling". Abstract: p. 22-23.

16. **A. Chesnokov**, **O. Lisovski**, **D. Bocharov**, **S. Piskunov**, and **Yu.F. Zhukovskii**, "Correlation between morphology of TiO₂ nanotubes and their photocatalytic abilities: ab initio study". Abstract: p. 28-29.

17. **A. Platonenko**, **Yu.F. Zhukovskii**, **S. Piskunov**, and **E.A. Kotomin**, "Ab initio simulations on interstitial oxygen atom in corundum". Abstract: p. 31.

VII. International Workshop "Advanced Methods of Oxide Materials Characterization" (Riga, Latvia, April, 2015).

18. **D. Gryaznov** and **E.A. Kotomin**, "Hybrid density functional calculations on bulk and surface properties of (La,Sr)FeO₃".

19. **A.I. Popov**, "VUV luminescence spectroscopy of perovskites".

VIII. E-MRS 2015 Spring Meeting (Lille, France, May, 2015).

20. **R.I. Eglitis**, "Towards a practical rechargeable 5 V Li ion battery". – Abstract: A.9.15.

21. **A. Chesnokov**, **O. Lisovski**, **D. Bocharov**, **S. Piskunov**, and **Yu.F. Zhukovskii**, "Ab initio simulations on pristine and doped TiO₂ anatase (101) nanotubes". – Abstract: B/P1.7.

22. G. Kaptagai, T.M. Inerbaev, A.T. Akilbekov, **Yu.A. Mastrikov**, and **E.A. Kotomin**, "Theoretical modeling of water adsorption on the fluorine-doped Co₃O₄ (111) surface". – Abstract: B/P2.23.

23. V.P. Savchyn, O.I. Aksimtyeva, Yu.Yu. Horbenko, I. Karbovnyk, and **A.I. Popov**, "Cathodoluminescence study of polystyrene–BaZrO₃ hybrid composites". – Abstract: C/P1.54.

24. **D. Bocharov**, M. Chollet, M. Krack, A. Kuzmin, J. Bertsch, D. Grolimund, and M. Martin, "Theoretical modeling of pristine and chromium-doped UO₂". – Abstract: F.1.4.

25. **Yu.F. Zhukovskii, A. Platonenko, S. Piskunov, and E.A. Kotomin**, “*Ab initio computer simulations of radiation defects in corundum*”. – Abstract: G.2.2.
26. **V.M. Lisitsyn, L.A. Lisitsyna, E.A. Kotomin, A.I. Popov, and J. Maier**, “*The peculiarities of the excitonic mechanism of defect formation and stabilisation in fluorides*”. – Abstract: G.2.3.
27. **A.Ch. Lushchik, Ch.B. Lushchik, A.I. Popov, K. Schwartz, E. Shablonin, O. Sidletskiy, and E. Vasil'chenko**, “*Influence of complex impurity centers on radiation damage in wide-gap metal oxides*”. – Abstract: G.5.3.
28. **V.N. Kuzovkov, E.A. Kotomin, A.I. Popov, and R. Vila**, “*Kinetics of radiation-induced colloid formation in Al_2O_3 and NaCl crystals*”. – Abstract: G.6.4.
29. **S. Piskunov and R.I. Eglitis**, “*Ab initio calculations of F center in $SrZrO_3$ bulk and (001) surfaces as well as $SrTiO_3/BaTiO_3$ and $SrZrO_3/PbZrO_3$ (001) interfaces*”. – Abstract: G/P.3.
30. **Yu.A. Mastrikov, P.V. Vladimirov, V.A. Borodin, A. Gopejenko, Yu.F. Zhukovskii, E.A. Kotomin, and A. Möslang**, “*Interaction of yttrium and oxygen with vacancy clusters within bcc-Fe matrix*”. – Abstract: G/P.11.
31. **A.I. Popov, E.A. Kotomin, and J. Maier**, “*Analysis of the self-trapped hole center mobility and recombination in alkali halides and complex metal halides*”. – Abstract: G/P.20.
32. **I. Bolesta, I. Karbovnyk, I. Rovetskii, S. Velgosh, and A.I. Popov**, “*Morphological evolution of nanostructures in long-term annealed CdI_2 crystals*”. – Abstract: H/9P.39.
33. **M. Arrigoni, T.S. Bjørheim, E.A. Kotomin, and J. Maier**, “*First principles thermodynamics of oxygen vacancies in ultrathin films of $BaZrO_3$* ”. – Abstract: M.11.3.
34. **E. Heifets, E.A. Kotomin, R. Merkle, and J. Maier**, “*Ab initio study of $BiFeO_3$ stability*.” – Abstract: M/P.13.
35. **Yu.A. Mastrikov, E.A. Kotomin, R. Merkle, M.M. Kuklja, and J. Maier**, “*Ab initio modelling of oxygen vacancies formation and migration in the bulk and on the surface of complex perovskites for solid oxide fuel cell cathodes*”. – Abstract: M/P.31.
36. **V. Dimza, A.I. Popov, L. Kundzina, M. Kundzins, K. Kundzins, M. Livins, and M. Antonova**, “*Effects of Mn doping on dielectric properties of ferroelectric relaxor PLZT ceramics*”. – Abstract: M/P.61.
37. **A.U. Abuova, E.A. Kotomin, Yu. A. Mastrikov, T.M. Inerbaev, and A.T. Akilbekov**, “ *$LaMnO_3$ (001) surface doping with Ag and its catalytic effect on the oxygen reduction*”. – Abstract: N/P1.9.
38. **A. Usseinov, E.A. Kotomin, A.T. Akilbekov, Yu.F. Zhukovskii, J. Purans, and F. Abuova**, “*Hydrogen migration and stability in ZnO: Ab initio calculations*”. – Abstract: N/P2.27.
39. **E.A. Kotomin, M.M. Kuklja, D. Fuks, Yu.A. Mastrikov, and J. Maier**, “*Structural stability of complex perovskites for solid oxide fuel cells from first principles calculations*”. – Abstract: N/P2.35.
40. **R.I. Eglitis**, “*Point defects as well as (001), (011) and (111) surfaces in ABO_3 perovskites*”. – Abstract: O/P.18.

IX. International Conference NANOMEETING-2015 (Minsk, Belarus, May, 2015).

41. **Yu.N. Shunin, Yu.F. Zhukovskii, V.I. Gopeyenko, N. Burlutskaya, T. Lobanova-Shunina, and S. Bellucci**, “*CNTs- and GNRs-based electromagnetic and spintronic devices: Models and simulations*”.

X. 227th Electrochemical Society Meeting (Chicago, USA, May, 2015).

42. **T.S. Bjoerheim, E.A. Kotomin, and J. Maier**, “*Defect chemistry of CeO_2 surfaces from first principles and space charge theory*”. - Abstract: 1775.

XI. MMA2015 (Sigulda, Latvia, May, 2015).

43. **O. Dumbrajs** and **H. Kalis**, "On numerical simulation of nonstationary oscillations in gyrotrons".

XII. Platform for Advanced Scientific Computing Conference PASC15 (Zurich, Switzerland, June, 2015).

44. **D. Bocharov**, **M. Krack**, and **A. Kuzmin**, "EXAFS spectra interpretation using molecular dynamics and DFT simulations". – Abstract: M/P.13.

XIII. EuroNanoForum-2015 (Riga, Latvia, June, 2015).

45. **A.V. Bandura**, **R.A. Evarestov**, and **Yu.F. Zhukovskii**, "Comparative analysis of four-faceted [001]-oriented nanowires formed from TiO₂ rutile and SrTiO₃ cubic phases: Ab initio simulations".

46. **A. Chesnokov**, **O. Lisovski**, **S. Piskunov**, **D. Bocharov**, and **Yu.F. Zhukovskii**, "Photocatalytic properties of doped TiO₂ nanotubes: Prediction from first principles".

47. **R.I. Eglitis**, "Ab initio calculations of point defects as well as (001), (011) and (111) surfaces in ABO₃ perovskites".

48. **Yu.N. Shunin**, **V.I. Gopeyenko**, **N. Burlutskaya**, **T. Lobanova-Shunina**, **S. Bellucci**, and **Yu.F. Zhukovskii**, "Electromechanical properties of carbon-based nanocomposites for pressure and temperature nanosensors".

XIV. 20th International conference on Solid State Ionics (Keystone Colorado, USA, June, 2015).

49. **E.A. Kotomin**, **Yu.A. Mastrikov**, **R. Merkle**, **M.M. Kuklja**, and **J. Maier**, "First principles calculations of formation and migration of oxygen vacancies in the bulk and on surface of complex perovskites for solid oxide fuel cell cathodes". Abstract: D4.04.

50. **T.S. Bjorheim**, **E.A. Kotomin**, and **J. Maier**, "Defect chemistry of CeO₂ surfaces from first principles and space charge theory". Abstract: D8.07.

51. **M.M. Kuklja**, **E.A. Kotomin**, **D. Fuks**, **Yu.A. Mastrikov**, and **J. Maier**, "Structural stability of complex perovskites for solid oxide fuel cells from first principles calculations". Abstract: A2.01.

52. **M. Arrigoni**, **E.A. Kotomin**, **J. Maier** and **T.S. Bjorheim**, "First principles thermodynamics of oxygen vacancies in ultrathin films of BaZrO₃". Abstract: A2.04.

XV. 11th International Conference on Diffusion in Solids and Liquids DSL-2015 (Munich, Germany, June, 2015).

53. **V.N. Kuzovkov** and **E.A. Kotomin**, "Static and dynamic screening effects in diffusion-controlled self-assembly of charged nanoparticles". Abstract: p. 153.

XVI. 27th Joint Russian-German Workshop on ECRH and Gyrotrons (Greifswald, Germany, June, 2015).

54. **O. Dumbrajs** and **G.S. Nusinovich**, "Field formation in the interaction space of gyrotrons".

XVII. 28th International Conference on Defects in Semiconductors (Helsinki, Finland, July, 2015).

55. **D. Gryaznov**, **R. Merkle**, and **E.A. Kotomin**, "Hybrid density-functional calculations on oxygen vacancy behaviour in complex perovskite oxides". Abstract: p.22.

56. **R.I. Eglitis**, Ab initio calculations of SrTiO₃, BaTiO₃, PbTiO₃ and CaTiO₃ perovskite (001), (011) and (111) surfaces. Abstracts: p.30.

57. **R.I. Eglitis**, H. Shi and R. Jia, *First principles calculations of the diffusion and aggregation of F centers, as well as bulk and surface H centers in CaF₂, BaF₂ and SrF₂*. Abstracts: p.30.

58. **R.I. Eglitis** and **S. Piskunov**, *First principles hybrid DFT calculations of F centers in SrZrO₃ bulk and (001) surfaces, as well as SrTiO₃/BaTiO₃ and SrZrO₃/PbZrO₃ (001) interfaces*. Abstracts: p.30.

59. **R.I. Eglitis**, *Towards a practical rechargeable 5 Volt Li ion battery*. Abstracts: p.30.

XVIII. 16th International Conference on X-ray Absorption Fine Structure XAFS16 (Karlsruhe, Germany, August, 2015).

60. **D. Bocharov**, M. Krack, A. Kalinko, J. Purans, F. Rocca, S.E. Ali, and A. Kuzmin, "Ab initio molecular dynamics simulations of the Sc K-edge EXAFS of scandium trifluoride". Abstract: p. 107.

61. J. Purans, **S. Piskunov**, **D. Bocharov**, A. Kalinko, A. Kuzmin, and F. Rocca, "Local structure of perovskites ReO₃ and ScF₃ with negative thermal expansion: interpretation beyond the quasiharmonic approximation". Abstract: p. 141.

62. **D. Bocharov**, M. Chollet, M. Krack, J. Bertsch, D. Grolimund, M. Martin, A. Kuzmin, J. Purans, and **E.A. Kotomin**, "Interpretation of the U L3-edge EXAFS in uranium dioxide using molecular dynamics and density functional theory simulations". Abstract: p.153.

XIX. 6th International Conference Diffusion Fundamentals (Dresden, Germany, August, 2015).

63. J.R. Kalnins, **E.A. Kotomin**, and **V.N. Kuzovkov**, "Effective diffusion coefficient in one-dimensional heterogeneous solids: a comparison of continuous and discrete lattice models". Abstract: p.27.

64. **V.N. Kuzovkov**, **E.A. Kotomin**, **A.I. Popov**, and R. Vila, "Diffusion-controlled kinetics of metallic colloid formation in irradiated Al₂O₃, MgO and NaCl crystals". Abstract: p.30.

65. **V.N. Kuzovkov**, **G. Zvejnicks**, and **E.A. Kotomin**, " Diffusion and self-assembly of charged nanoparticles in polar media: a competition between short-range and long-range interactions". Abstract: p.31.

XX. 40th International conference on Infrared, Millimeter and Terahertz Waves (Hong Kong, August, 2015).

66. **O. Dumbrajs**, E.M. Khutoryan, and T. Idehara, "Hysteresis and frequency tenability of gyrotrons".

XXI. JA-EU-US RF Heating Technology Workshop (Tokyo, Japan, August – September, 2015).

67. **O. Dumbrajs**, E.M. Khutoryan, and T. Idehara, "Hysteresis and frequency tenability of gyrotrons".

XXII. Solid state electrochemistry workshop (Roggenburg, Germany, September, 2015).

68. **E.A. Kotomin**, **D. Gryaznov**, and **Yu.A. Mastrikov**, "Defects in complex perovskites for electrochemical applications".

XXIII. E-MRS 2015 Fall Meeting, Symposium J (Ferroic perovskites for advanced materials) (Warsaw, Poland, September, 2015).

69. **D. Gryaznov**, M. Arrigoni, **E.A. Kotomin**, and **A.I. Popov**, "Hybrid DFT calculations of the electronic and phonon properties of defects in perovskite oxides". Abstract: J6.

XXIV. 3rd International School-Conference on Atomistic Simulations of Functional Materials (Moscow, Russia, October 2015).

70. E.A. Kotomin, "Ab initio calculations of defects in complex perovskites for energy applications".

XXV. 11th International Conference "Functional Materials and Nanotechnologies" FM&NT-2015 (Vilnius, Lithuania, October, 2015).

71. Yu.N. Shunin, S. Bellucci, Yu.F. Zhukovskii, T. Lobanova-Shunina, N Burlutskaya, and V.I. Gopeyenko, "Modeling and simulation of CNTs- and GNRs-based nanocomposites for nanosensor devices". Abstract: p. 45.

XXVI. COST Action CM1104 "Reducible oxides" meeting (Salzburg, Austria, October, 2015).

72. E.A. Kotomin, Yu.A. Mastrikov, M.M. Kuklja, D. Fuks, and J. Maier, "Structural stability of complex perovskites for solid oxide fuel cells: first principles calculations". Abstract: p. 15

73. Yu.A. Mastrikov, E.A. Kotomin, R. Merkle, M.M. Kuklja, and J. Maier, "Ab initio modeling of oxygen vacancy on LSCF surface". Abstract: p. 16

XXVII. First Workshop on Research into Nuclear Fuel in Europe and Materials Modeling and Simulation for Nuclear Fuels Workshop (Karlsruhe, Germany, November, 2015).

74. M. Krack, D. Bocharov, and A. Kuzmin, "Analysis of U L3-edge X-ray absorption spectra for uranium dioxide based on molecular dynamics simulations". Abstract: P.5.3.

XXVIII. Advances in Materials and Processing Technologies conference AMPT (Madrid, Spain, December, 2015).

75. M. Krack, D. Bocharov, and A. Kuzmin, "Structural and electronic properties of chromium doped uranium dioxide". Abstract: RE 7.
